NASA/TM—2000-209418

Assessments of Low Cycle Fatigue Behavior of Powder Metallurgy Alloy U720

Timothy P. Gabb
Glenn Research Center, Cleveland, Ohio

Peter J. Bonacuse
U.S. Army Research Laboratory, Glenn Research Center, Cleveland, Ohio

Louis J. Ghosn
Glenn Research Center, Cleveland, Ohio

Joseph W. Sweeney
Gilcrest Electric Company, Brook Park, Ohio

Amit Chatterjee and Kenneth A. Green
Allison Engine Company, Indianapolis, Indiana

March 2000

The NASA STI Program Office . . . in Profile

Since its founding, NASA has been dedicated to the advancement of aeronautics and space science. The NASA Scientific and Technical Information (STI) Program Office plays a key part in helping NASA maintain this important role.

The NASA STI Program Office is operated by Langley Research Center, the Lead Center for NASA's scientific and technical information. The NASA STI Program Office provides access to the NASA STI Database, the largest collection of aeronautical and space science STI in the world. The Program Office is also NASA's institutional mechanism for disseminating the results of its research and development activities. These results are published by NASA in the NASA STI Report Series, which includes the following report types:

- TECHNICAL PUBLICATION. Reports of completed research or a major significant phase of research that present the results of NASA programs and include extensive data or theoretical analysis. Includes compilations of significant scientific and technical data and information deemed to be of continuing reference value. NASA's counterpart of peer-reviewed formal professional papers but has less stringent limitations on manuscript length and extent of graphic presentations.

- TECHNICAL MEMORANDUM. Scientific and technical findings that are preliminary or of specialized interest, e.g., quick release reports, working papers, and bibliographies that contain minimal annotation. Does not contain extensive analysis.

- CONTRACTOR REPORT. Scientific and technical findings by NASA-sponsored contractors and grantees.

- CONFERENCE PUBLICATION. Collected papers from scientific and technical conferences, symposia, seminars, or other meetings sponsored or cosponsored by NASA.

- SPECIAL PUBLICATION. Scientific, technical, or historical information from NASA programs, projects, and missions, often concerned with subjects having substantial public interest.

- TECHNICAL TRANSLATION. English-language translations of foreign scientific and technical material pertinent to NASA's mission.

Specialized services that complement the STI Program Office's diverse offerings include creating custom thesauri, building customized data bases, organizing and publishing research results . . . even providing videos.

For more information about the NASA STI Program Office, see the following:

- Access the NASA STI Program Home Page at ***http://www.sti.nasa.gov***

- E-mail your question via the Internet to help@sti.nasa.gov

- Fax your question to the NASA Access Help Desk at (301) 621-0134

- Telephone the NASA Access Help Desk at (301) 621-0390

- Write to:
  NASA Access Help Desk
  NASA Center for AeroSpace Information
  7121 Standard Drive
  Hanover, MD 21076

NASA/TM—2000-209418

Assessments of Low Cycle Fatigue Behavior of Powder Metallurgy Alloy U720

Timothy P. Gabb
Glenn Research Center, Cleveland, Ohio

Peter J. Bonacuse
U.S. Army Research Laboratory, Glenn Research Center, Cleveland, Ohio

Louis J. Ghosn
Glenn Research Center, Cleveland, Ohio

Joseph W. Sweeney
Gilcrest Electric Company, Brook Park, Ohio

Amit Chatterjee and Kenneth A. Green
Allison Engine Company, Indianapolis, Indiana

National Aeronautics and
Space Administration

Glenn Research Center

March 2000

Acknowledgments

The authors wish to acknowledge the extensive statistical assistance provided by Dennis Keller of RealWorld Quality Systems

Available from

NASA Center for Aerospace Information
7121 Standard Drive
Hanover, MD 21076
Price Code: A03

National Technical Information Service
5285 Port Royal Road
Springfield, VA 22100
Price Code: A03

Assessments of Low Cycle Fatigue Behavior of Powder Metallurgy Alloy U720

Timothy P. Gabb
National Aeronautics and Space Administration
Glenn Research Center
Cleveland, Ohio

Peter J. Bonacuse
U.S. Army Research Laboratory
Glenn Research Center
Cleveland, Ohio

Louis J. Ghosn
National Aeronautics and Space Administration
Glenn Research Center
Cleveland, Ohio

Joseph W. Sweeney
Gilcrest Electric Company
Brook Park, Ohio

Amit Chatterjee and Kenneth A. Green
Allison Engine Company
Indianapolis, Indiana

ABSTRACT: The fatigue lives of modern powder metallurgy disk alloys are influenced by variabilities in alloy microstructure and mechanical properties. These properties can vary as functions of variables the different steps of materials/component processing: powder atomization, consolidation, extrusion, forging, heat treating, and machining [1–4]. It is important to understand the relationship between the statistical variations in life and these variables, as well as the change in life distribution due to changes in fatigue loading conditions. The objective of this study was to investigate these relationships in a nickel-base disk superalloy, U720, produced using powder metallurgy processing. Multiple strain-controlled fatigue tests were performed at 538 °C (1000°F) at limited sets of test conditions. Analyses were performed to: 1) assess variations of microstructure, mechanical properties, and LCF failure initiation sites as functions of disk processing and loading conditions; and 2) compare mean and minimum fatigue life predictions using different approaches for modeling the data from assorted test conditions.

Significant variations in life were observed as functions of the disk processing variables evaluated. However, the lives of all specimens could still be combined and modeled together. The failure initiation sites for tests performed at a strain ratio $R_\varepsilon=\varepsilon_{min}/\varepsilon_{max}$ of 0 were different from those in tests at a strain ratio of –1. An approach could still be applied to account for the differences in mean and maximum stresses and strains. This allowed the data in tests of various conditions to be combined for more robust statistical estimates of mean and minimum lives.

Introduction

The low cycle fatigue (LCF) lives, life frequency distributions, and predominant failure modes of powder metallurgy disks can be influenced by material processing details including powder characteristics, consolidation, extrusion, forging, heat treating, and machining processing parameters, [1–4]. Processing history also introduces dependencies of LCF behavior on location in a disk. These effects on fatigue behavior can change as functions of service/testing conditions: temperatures, times, imposed stresses/strains. It is often not possible to assess these issues with a statistically significant number of fatigue specimen tests in many conditions producing lives $>10^4$ cycles, due to testing costs, time, and material constraints. Yet many applications require such design lives. The objective of this work was to study the LCF life behavior of the powder metallurgy (PM) disk alloy U720 in many tests at limited, long life ($>10^4$ cycles) test conditions. The LCF behavior as functions of several processing variables (disk and specimen location) was first assessed. Life distributions and minimum life estimates were then evaluated for each selected test condition when pooling data. Minimum life estimates were also performed when combining data of different test conditions.

Material and Procedures

Production-scale PM U720 disk material, previously described [5], was supplied by Allison Engine Company. The powder for this material was atomized in argon. After screening and blending, the powder was hot isostatic pressed, extruded, and then cluster forged. The disks were separated from the forged clusters, and given a subsolvus solution, oil quench, and two step aging heat treatment. Specimens with uniform gages of 0.635cm (0.25in) diameter were machined from the rims of an outer disk (#16) of one cluster and a center disk (#43) of another cluster forging (Fig. 1). The specimens were grouped together for each disk, in hopes of minimizing location effects. However, tests were designed to allow evaluations of the following variables: disk (D), radial location (R) and vertical location within disk (V). A 2×3×2 full factorial statistical test matrix with repetitions was used. Two prime test conditions were selected, each estimated to have mean lives of near 200,000 cycles at 538 °C (1000 °F). A total strain range ($\Delta\varepsilon_t$) of 0.75 percent was used with a strain ratio ($R_\varepsilon=\varepsilon_{min}/\varepsilon_{max}$) equal to 0 in one series of 20 tests. A total strain range ($\Delta\varepsilon_t$) of 0.90 percent was used with a strain ratio ($R_\varepsilon=\varepsilon_{min}/\varepsilon_{max}$) equal to –1 in the other series of 20 tests. To reduce testing time each experiment was performed in two stages. First, the test was conducted in strain control using a triangular waveform at a frequency of 0.33 hertz. After cycling for 24 hours, tests were continued to failure using a triangular waveform in load control at a frequency of 10 hertz. For each test, the load control settings were adjusted to reproduce the stabilized maximum and minimum loads generated during the previous strain cycling at 0.33 hertz. All tests were continued to failure and fractographic evaluations were performed on all specimens. Metallographic analyses were performed on selected specimens spanning the range of process variables and test conditions. For the fatigue life relationships, least squares multiple linear regressions were performed using forward step-wise inclusion of independent variables, requiring an F-ratio to enter of 2.0. Adjusted correlation coefficients (r_{adj}^2) and root mean square standard deviations were used to compare among the different resulting relationships. The F test for lack of fit and graphical residual analyses were also performed to check the aptness of each model.

Results and Discussion

Overview

The typical microstructure of selected test specimens is shown in Fig. 2. The mean grain size ranged from ASTM 12 to 12.5. Primary γ' particles of 1–3 μm diameter took up an area fraction of 14 to 18 percent. Finer cooling γ' precipitates of 0.08–0.13 μm diameter and very fine aging γ' were in far greater abundance. The fatigue test results are listed (Tables 1,2). Twenty fatigue tests were performed at each of the two prime test conditions. Cyclic lives in these tests were from 53,269 to 446,550 cycles. Eight additional screening tests were performed at $R_\varepsilon = -1$ with higher $\Delta\varepsilon_t$ of 0.92–1.0 percent, giving cyclic lives of 10,017 to 473,868 cycles. The predominant failure initiation sites varied with R_ε. Tests performed with $R_\varepsilon = 0$ predominantly failed from cracks at elongated clusters of oxide inclusions, as shown in Fig. 3. These inclusions appeared to be of the class generally referred to as Type II reactive inclusions [1,4]. No surrounding reaction zones containing phases other than the typical γ, γ', and carbides were identified at these Type II inclusions. However, these inclusions were often surrounded by several large grains having less primary γ' apparent. Tests performed with $R_\varepsilon = -1$ principally failed from cracks emanating from large, sheared grains ("grain facet failures") or at pores, as shown in Fig. 4. The failures initiated internally in about 75 percent of all tests.

Evaluations of Response Variations Due to Processing/Location Variables

Three processing and location variables were assessed: disk forging and location within the forging cluster (D), specimen radial location (R), and specimen vertical location (V). D was treated as a continuous variable at two levels of #16 and #43, and R was treated as a continuous variable at three levels of 6.36, 7.95, and 9.54 cm (2.51, 3.13, and 3.76 in.). V was treated as a discrete variable at two levels of 1 (adjacent to the disk top surface) and –1 (adjacent to the bottom). Microstructure, strength, and life responses at each of the two prime test conditions were evaluated. Lives at the two test conditions are plotted versus the three processing/location variables of disk, radial distance in the disk, and vertical position in the disk, Fig. 5. No direct, simple dependencies are evident in these scatter plots. Assessments of the combined effects of the variables were then performed using multiple linear regression analyses, with logarithm of fatigue life, maximum failure defect length, and minimum failure defect length at each prime test condition as the dependent variables. Similar analyses were also performed using mean grain size, standard deviation of grain size, and maximum grain length as the dependent variables, as measured from the metallographic sections of test specimens. The resulting derived regression equations which had statistically significant dependencies ($r^2_{adj}>0.25$) are summarized in Table 3. Positive and negative signs indicate the signs of the estimated regression constants for each significant independent variable. The dependent variables of ln life at each prime test condition, 0.1 percent yield strength (measured from the first fatigue cycle in tests at $R_\varepsilon = 0$), and mean grain size had statistically significant relationships with the D,R,V variables. In both of the prime test conditions, ln(life) increased with decreasing R and increasing D*R. This may be somehow related to the finer grain size (increasing ASTM grain size number) observed with decreasing R. However, the analyses did not indicate this was simply due to increasing yield strength with finer grain size, as in a traditional Hall-Petch relationship. Instead, yield strength was shown to decrease with decreasing R. The physical significance of the D*R term is also unclear.

The correlation coefficients $r^2>0.25$ for these regression equations imply significant relationships exist between the responses and the processing/location variables. However, the correlation coefficients are relatively low ($r^2<0.65$), indicating these relationships have relatively poor predictive capabilities. Therefore, while recognizing the processing/location variables do account for some of the scatter in the data, the data will be combined to make useful life predictions.

Assessments of Life Relationships and Distributions At Each Prime Test Condition

Plots of estimated cumulative probability versus life are shown in Fig. 6 for each prime test condition. Normally distributed data should lie along a straight line at a constant slope in these probability plots of Fig. 6. Three-parameter Weibull distribution curves were also used to model the probability of life Pr(N) using the equation [7]:

$$Pr(N) = 1-\exp[-\{(N-a)/b\}^m],$$

where a, b, and m are empirical constants fit by regression. Weibull distributed data should lie along a straight line when the Weibull function of estimated cumulative probability:

$$\ln(\ln(1-Pr(N))^{-1})$$

is plotted versus $\ln(N_f)$ as in Fig. 6. An alternative approach is to transform the life data into a more normally distributed parameter using a transformation function. Probability plots of a logarithm transformation of life [6], $\log(N_f)$, are shown in Fig. 7.

Selection among these different approaches of treating life frequency distributions was based in part on the constancy of slope (linearity) of the probability plots. The abilities of each approach in generating robust estimates of mean and minimum lives were also considered. Mean and minimum lives needed to be assessed using a consistent approach that was not overly sensitive to single data points. Estimates of mean and minimum (Pr = .00135 = "-3σ") lives were calculated for each prime test condition using each of the frequency distribution assumptions described above. In order to assess the sensitivity of the approach to single data points, mean and minimum lives for each prime condition were calculated using all 20 tests and then using 19 tests, after omitting the lowest life test.

The results are compared in Table 4 and Fig. 8. An assumption of normally distributed lives produced reasonable estimates of mean life. However, the estimates of minimum lives at a probability Pr = 0.00135 were negative and invalid. This was a consequence of the non-linear probability curves. Fitting Weibull equations to model the life distributions produced more meaningful estimates of both mean and minimum lives for each prime test condition. However, comparison of Weibull curve minimum life estimates with the lowest life test for each prime condition indicated this approach was highly sensitive to the lowest life test, and was not always lower than the observed data. Estimated minimum life tracked unreasonably close to the lowest life test. This response was illustrated by removing the lowest life test for each prime data set.

The log N_f transformation of the life data was selected for subsequent evaluations. This transformation produced more linear cumulative probability curves. The mean and minimum life estimates using the transformed data showed a more reasonable influence of the lowest life test than the other approaches, and the minimum life estimates were always lower than the observed data. For each prime test condition, the estimated mean and minimum lives moderately increased after removal of the lowest life test. Based on these findings, the log N_f transformation was selected for further evaluations.

Evaluation of All Available Data in General Stress/Strain-Life Equations

All available test data on this material was now combined for a more general life equation. Allison Engine Company had previously run LCF tests on specimens from the same group of disks at higher strain ranges with $R_\varepsilon = 0$ and –1, and also load controlled high cycle fatigue (HCF) tests at $R_\varepsilon = 0$ and –1. All data was now combined to produce a combined life relationship.

An evaluation was first performed on all available LCF data, where the test variables $\Delta\varepsilon_t$ and R_ε were consistently held constant during testing. A total of 68 LCF tests were analyzed. Stepwise multiple linear regression and residual analyses indicated the equation:

$$\log N_f = C_o + C_1 R_\varepsilon + C_2/\Delta\varepsilon_t^{\,3} + C_3 R_\varepsilon /\Delta\varepsilon_t^{\,3}$$

was suitable for fitting the combined LCF data (r^2_{adj}=0.847).

All available LCF and HCF data were now analyzed together. Recall that tests at a given $\Delta\varepsilon_t$ performed with $R_\varepsilon = 0$ had different mean and maximum strains and stresses than those for $R_\varepsilon = -1$ (Tables 1,2). In a like manner, HCF tests at a given $\Delta\sigma$ performed with $R_\sigma = 0$ had different mean and maximum strains and stresses than those for $R_\sigma = -1$. Stepwise multiple linear regression was performed to find the most significant variables among $\Delta\varepsilon_t$, R_ε, $\Delta\sigma$, R_σ, σ_{max}, and σ_{mean} which influenced log life. In the LCF test cases, $\Delta\varepsilon_t$, R_ε, σ_{max}, and σ_{mean} were taken at half of cyclic life. In the HCF test cases, $\Delta\varepsilon_t$ was approximated as $\Delta\sigma/E$ with E = 194.1 GPa (28.15×10^6 psi), as these tests were nominally elastic with strain not monitored. The independent variables $\Delta\varepsilon_t$ and σ_{max} were found to be the most significant parameters influencing log life. Multiple linear regression and residual analyses indicated an equation of the form:

$$\log N_f = C_o + C_1 \log \Delta\varepsilon_t + C_2 \log \sigma_{max} + C_3 \log \Delta\varepsilon_t \log \sigma_{max}$$

was suitable for fitting the combined data ($r^2_{adj} = 0.841$).

Three analytical approaches combining strain and stress effects were then assessed. A simple Smith-Watson-Topper effective stress parameter [8] was employed using the equation:

$$\sigma_{SWT} = (\sigma_{max}\, \Delta\varepsilon_t E/2)^{1/2} .$$

A Walker equivalent stress parameter [9] was also used, with the equation:

$$\sigma_W = \sigma_{max} (\Delta\varepsilon_t E/\sigma_{max})^m ,$$

where m is an additional empirical material constant which must be regressed using the life data. Generalized equations were fit by least squares multiple linear regression combined with residual analyses to the combined data sets using log N_f transformed lives versus σ_{SWT} and σ_W. A value of m = 0.53 gave the best fit of σ_W to the life data. Fatigue life has often been related to applied strains and stresses using a power law of the general form, $N_f=C_o\ (\varepsilon,\sigma)^{C1}$. So logarithms and powers of each of these variables were also assessed using equations of the forms:

$$\log N_f = C_o+C_1\log \sigma \text{ and } \log N_f=C_o+C_1\sigma^{C2}.$$

For both σ_{SWT} and σ_W, equations of the form:

$$\log N_f = C_o+C_1\log \sigma$$

were found to be most suitable.

A strain-based Basquin-Coffin-Manson type equation was also applied [10], in which the total strain range was separated into elastic and plastic components:

$$\Delta\varepsilon_{corr} = \Delta\varepsilon_{el,corr} + \Delta\varepsilon_{pl} = B(N_f)^b + C(N_f)^c$$

A correction similar to the Walker approach was used to modify the elastic strain range for stress ratio effects:

$$\Delta\varepsilon_{el,corr} = \frac{\Delta\sigma}{E}(2 + R_\sigma)^m$$

This equation reduces to $\Delta\sigma/E$ for fully reversed experiments (R = -1) and increases the equivalent elastic strain range for larger stress ratios. The resulting strain-life equation was fit using a linear regression approach where the logarithms of the elastic strain range and plastic strain range were each separately fit to log life. As the plastic strain range is a calculated value:

$$\Delta\varepsilon_{pl} = \Delta\varepsilon_t - \Delta\sigma/E$$

and is vanishingly small (at or near the resolution threshold of the strain measurement instrumentation) for many of the experiments, only the highest strain range experiments were used to compute the constants C and c.

The resulting four generalized life equations are compared in Table 5 with the corresponding root mean square standard deviations and correlation coefficients. Actual lives are compared to lives estimated using the log N_f = f(log $\Delta\varepsilon_t$,log σ_{max}) equation in Fig. 9. These generalized life equations are more versatile for estimating lives at various stress/strain conditions, but they

introduced more variability than that previously calculated at each of the prime test conditions. The standard deviations previously calculated using data generated only at each prime test conditions with the log N_f life transformation are included for comparison in Table 5. At each condition, the equations' rms standard deviations were 25–60 percent higher than those previously calculated using the prime data sets. The additional HCF data appeared to have more scatter in life, as should be expected, and probably contributed to the increased standard deviations. Another inherent source of this additional variability could be remnant effects on life due to differences in stresses and strains which were not sufficiently compensated with the $\Delta\varepsilon$ and $\Delta\sigma$ variables using the combined approaches selected. Application of other combined stress/strain compensation approaches might reduce such variability. However, a major source of the additional variability of the combined data was provided by a low life outlier LCF test at $\Delta\varepsilon_t = 0.92$ percent having a life of only 10,017 cycles, as will be discussed below.

Minimum life estimates of the generalized life equations were lower and more conservative than those calculated using data only generated at the prime test conditions. Mean and minimum life estimates of the generalized life equations are compared at each of the prime test conditions to those previously calculated using only data generated at these conditions (Table 5). Mean life estimates of the life equations are similar to those previously calculated using the prime data sets. Minimum life estimates of the generalized life equations were lower than those previously calculated, by 38–73 percent.

Additional evaluations were performed to assess the sensitivities of the generalized equations to outlier data points. Regression analyses indicated an LCF test at $\Delta\varepsilon_t = 0.92$ percent having a life of only 10,017 cycles was a low life outlier, with a large influence on the regressions. This data point was removed, and the generalized life equations were again regressed with the combined data set. The resulting life estimates are also included (Table 5). For both equations, standard deviations of the combined data set decreased substantially. Mean and minimum life estimates consequently increased, with larger increases in the $R_\varepsilon = -1$ life estimates. This indicated low life outlier data points could influence general life equations and minimum life estimates.

Defect Initiation Sites and Their Influence on Life Estimates

The observed failure initiation sites in this powder material ranked by occurrence were Type II inclusions, faceted grain failures, and pores. While faceted grains can be considered inherent features of the microstructure, the Type II inclusions and pores are clearly undesirable defects, that might reduce the fatigue lives by orders of magnitudes. Therefore, further evaluations of failures initiating at these undesirable defects were briefly conducted. The maximum length and minimum depth of these defects initiating failure were measured for every specimen tested in the two prime test conditions. Scatter plots of life versus defect length and depth are shown for each test condition, Fig. 12. No consistent or significant trends were observed using these chosen simple defect parameters. However, other defect parameters incorporating projected area, aspect ratio, and orientation could possibly have more significant relationships to life.

The proportion of cyclic life taken up in initiating cracks at these defects was then estimated for these cases. The number of fatigue cycles necessary to grow cracks initiating from the defects to final fracture was calculated using a fracture mechanics framework. Actual aspect ratios of the

inclusions or pores initiating the crack as well as the corresponding distance to the free surface were measured from the fracture surfaces and used in the propagation life calculations. The stress intensity factor solution of an internal elliptical crack near a free surface was employed in the crack propagation code FASTRAN II [11], developed at NASA Langley Research Center. But as the crack reached the free surface, the stress intensity factor solution was switched to an elliptical crack in a round specimen, and the analysis was continued until specimen fracture. The applied remote stress ranges assumed in the calculations were the experimentally measured stress ranges at half of the cyclic life. The crack propagation law employed in the analysis used the equation:

$$da/dn=9.9x10^{-9}(\Delta K_{eff})^{2.1}.$$

based on data generated from compact tension specimens of this material tested at 1000 °F.

Since the stress intensity factor ranges (ΔK) incorporate all the major geometric features of the defects as well as locations, the total lives were correlated with the initial ΔK, at a_0 (see Fig. 13). A clear trend of decreasing total cyclic life is observed with increasing ΔK, but with a large scatter in the data. The propagation lives were calculated and plotted in Fig. 14 as a function of the initial ΔK. While the propagation lives were estimated to be between 10,000 to 30,000 cycles in these tests, the total lives were in the range of 10^5 to 10^6 cycles. As a refinement, only the initiation lives (total life – propagation life) were plotted as a function of the initial ΔK (see Fig. 15), with still no great improvement in the scatter. The percent of the calculated propagation lives were only 5–10 percent of the total lives (as see Fig. 16), except for the two outliers where the propagation lives are 20 and 40 percent for an inclusion and a pore, respectively. Hence no pronounced reduction in the scatter was observed with only the initiation lives. Refinements using actual crack growth data generated on this material in vacuum for the internal crack propagation phase and in air for the subsequent surface connected crack growth could change the crack propagation life estimates. Furthermore, using crack propagation laws generated from highly constrained specimens such as the K_b specimen [12] simulating the actual condition that the defects are subjected to, might also improve the estimated propagation lives. However, it is clear that these defects can withstand a large number of cycles before initiating cracks in the prime, long life test conditions evaluated. Predictions of overall life in this material could benefit from determining the initiation lives associated with these defects, as functions of defect size, location, and test conditions.

Summary of Results and Conclusions

Summary of Results

Fatigue tests of powder metallurgy U720 were performed at 538 °C (1000 °F) principally using two prime test conditions with multiple replicates. Statistical, microstructural, and failure analyses were performed to assess life response and relationships.

1. Several significant property correlation's as functions of processing/location variables were identified, however the correlation's had poor predictive capabilities.
2. Data were successfully combined at each of the two prime test conditions for life distribution assessments, in spite of the processing/location dependencies.

3. Predominant failure initiation sites varied between the two prime test conditions, however the data were combined after using a logarithmic life transformation to produce generalized life equations including both LCF and HCF test results.
4. The generalized equations fitted to the combined data gave lower, more conservative minimum life estimates than those generated only from data at the prime test conditions.
5. Crack propagation life calculations using fractographic measurements indicated near 90 percent of cyclic life was required to initiate cracks at inclusions or pores in the prime test conditions.

Conclusions

1. Disk alloy processing/location variables can influence fatigue lives in certain conditions, and their influences can account for some of the statistical scatter observed in life.
2. Fatigue life for these conditions can be treated as normally distributed, after appropriate transformations such as log life.
3. Data generated for these conditions at different R ratios and test control modes can be combined using a generalized approach employing total strain range and maximum stress, using either direct multiple linear regression equations or combined stress-strain parameters which account for different strain ranges and maximum stresses.
4. Generalized life equations using the logarithm of life can be generated to allow life estimation in other stress and strain conditions, which give reasonable, conservative mean and minimum life estimates.
5. General improvements in the fatigue life of this material for these conditions would require improvements in the control of Type II inclusions, pores, and grain size variability. An understanding of the crack initiation characteristics of these defects could also allow more accurate life predictions of the current material.

References

[1] D.R. Chang, D.D. Charger, and R.A. Sprague, in Superalloys 1984, TMS-AIME, Warrendale, PA, 1984, pp. 245–252.

[2] R.D. Kissinger, in Superalloys 1996, TMS-AIME, Warrendale, PA, 1996, pp. 687–696.

[3] P.A. Domas, "Elevated Temperature Component Fatigue Robustness – An Holistic Approach", AGARD-CP-569, AGARD, March 1996.

[4] E.S. Huron, and P.G. Roth, in Superalloys 1996, TMS-AIME, Warrendale, PA, 1996, pp. 359–368.

[5] K.A. Green, J.A. Lemsky, and R.M. Gasior, in Superalloys 1996, TMS-AIME, Warrendale, PA, 1996, pp. 697–704.

[6] G.M. Sinclair, and T.J. Dolan, "Effect of Stress Amplitude on Statistical Variability in Fatigue Life of 75S-T6 Aluminum Alloy", Transactions of the ASME, vol. 19, July 1953, pp. 867–872.

[7] W. Weibull, "A Statistical Distribution Function of Wide Applicability," Journal of Applied Mechanics, 1951.

[8] K.N. Smith, P. Watson, and T.H. Topper, "A Stress-Strain Function for the Fatigue of Metals", Journal of Materials, vol. 5, no. 4, Dec. 1970, pp. 767–778.

[9] K. Walker, "The Effect of Stress Ratio During Crack Propagation and Fatigue for 2024-T3 and 7075-T6 Aluminum", Effects of Environment and Complex Load History on Fatigue Life, ASTM STP 642, American Society for Testing and Materials, West Conshohocken, PA, 1970, pp. 1–14.

[10] S.S. Manson, Thermal Stress and Low-cycle Fatigue, McGraw-Hill, New York, 1966, pp. 141.

[11] J.C. Newman, FASTRAN-II – A Fatigue Crack Growth Structural Analysis Program", NASA TM–104159, Feb. 1992.

[12] R.H. Vanstone, and T.L. Richardson, "Potential-Drop Monitoring of Cracks in Surface-Flawed Specimens", Automated Test Methods for Fracture and Fatigue Crack Growth, ASTM STP 877, American Society for Testing and Materials, West Conshohocken, PA, 1985, pp. 148–166.

Table 1 – *LCF Test Results at R_ε=0*

Total Strain Range	Inelastic Strain	Elastic Strain	Max Stress	Min Stress	Modulus	Failure Life	Failure Init.	Max. Length	Width	Minimum Depth
$\Delta\varepsilon_t$-mm/mm	mm/mm	mm/mm	MPa	MPa	GPa	N_f	Site	μm	μm	μm
0.0075	0	0.0075	1147	-303	193	168376	Type II: Al-oxide	69.6	31.1	37
0.0075	0.0001	0.0074	1126	-304	194	186264	Facet, 1 grain	83.8	31.4	3.3
0.0075	0.0001	0.0074	1126	-292	197	172076	Type II: Al-oxide	47.4	5.2	1763
0.0075	0.0001	0.0074	1134	-290	198	159414	Type II: Al-oxide	204.3	46.1	487
0.0075	0.0001	0.0074	1143	-271	197	312603	Pores, clustered	54.5	17.9	37
0.0075	0.0001	0.0074	1103	-314	191	53269	Type II: Al,Mg,Si-oxide	139	80.8	1409
0.0075	0	0.0075	1149	-330	197	233639	Type I: Zr-oxide	44.7	39.3	240.8
0.0075	0.0001	0.0074	1107	-343	198	192204	Type II: Al-oxide	231.1	43.8	1352
0.0075	0.0001	0.0074	1117	-303	192	179199	Type II: Al,Ti –oxide	93.3	69.4	2040
0.0075	0.0001	0.0074	1089	-316	190	331636	Type II: Al-oxide	136.5	35.3	891.7
0.0075	0	0.0075	1104	-356	194	446550	Pores, clustered	36.8	19.1	69.8
0.0075	0.0002	0.0073	1130	-350	203	148743	Type II: Al-oxide	48.3	11.9	522.4
0.0075	0.0001	0.0074	1086	-387	199	277463	Type II: Al,Ti –oxide	95.4	15.9	2135.6
0.0075	0.0001	0.0074	1131	-303	194	186664	Type II: Al,S –oxide	108.5	14.7	92.2
0.0075	0.0001	0.0074	1115	-330	194	194703	Type II: Al,Si –oxide	231.4	22.7	226
0.0075	0.0002	0.0073	1113	-359	199	149486	Type II: Al-oxide	237.2	34.8	1560
0.0075	0.0001	0.0074	1127	-303	194	150470	Type II: Ti,Al –oxide	119.4	52.8	1388
0.0075	0.0001	0.0074	1077	-370	194	167624	Type II: Al,Ca,Ti -oxide	242	29.4	487.5
0.0075	0.0001	0.0074	1103	-343	197	259434	Type II: Al-oxide	27.3	4.1	1838
0.0075	0	0.0075	1103	-368	197	345840	Facet, 1 grain	61.7	34.3	208.7

Table 2 – *LCF Test Results at R_ε=-1*

Total Strain Range	Inelastic Strain	Elastic Strain	Max Stress	Min Stress	Modulus	Failure Life	Failure Init.	Max. Length	Width	Minimum Depth
$\Delta\varepsilon_t$-mm/mm	mm/mm	mm/mm	MPa	MPa	GPa	N_f	Site	μm	μm	μm
0.01	0.0004	0.0096	966	-962	199	42115	Pore	33.7	15.4	4.8
0.0095	0.0001	0.0094	897	-925	194	141272	Facet, 2 grains	170.1	55.1	2269
0.0092	0.0001	0.0091	868	-898	194	161486	Type I: Zr-oxide	31.4	18.6	3.9
0.0092	0.0002	0.009	881	-896	196	10017	Pore	19.6	16.2	1.3
0.0092	0.0002	0.009	924	-900	203	473868	Pores, cluster	42	10.5	41.2
0.0092	0.0002	0.009	912	-871	197	144567	Type I, Zr-oxide	33	18.9	4.4
0.0092	0.0002	0.009	899	-901	200	134510	Facet	51.9	26	28.8
0.0092	0.0001	0.0091	927	-860	194	77140	Type I: Zr-oxide	80.7	47.7	3.9
0.009	0.0001	0.0089	843	-922	197	309714	Facet, 1 grain	24.5	19.2	974
0.009	0	0.009	852	-905	196	438466	Facet, 1 grain	32	20.4	1494
0.009	0.0001	0.0089	881	-840	194	253263	Pores, clustered	36.6	3.9	1250
0.009	0.0001	0.0089	858	-871	193	446557	Facet, 1 grain	50.5	18.6	1440
0.009	0	0.009	868	-872	197	324410	Facets, 3 grains	177.6	47.1	2578.1
0.009	0.0001	0.0089	869	-855	194	325270	Facet, 1 grain	59.8	38.8	1925.4
0.009	0	0.009	892	-867	194	299422	Facets, 2 grains	57.7	43	327
0.009	0.0001	0.0089	893	-841	194	340120	Pores, 2 adjoining	44.2	17.8	31
0.009	0.0001	0.0089	845	-858	192	183923	Pores, clustered	40.4	14.4	23.1
0.009	0	0.009	865	-895	197	231456	Facet, 1 grain	39.7	32.5	83.3
0.009	0.0001	0.0089	868	-911	200	255906	Type II: Al-oxide	31.9	4.8	67.7
0.009	0.0001	0.0089	898	-916	203	199260	Facet, 1 grain	66.4	44.5	1920
0.009	0	0.009	845	-926	197	217992	Pores, 2 adjoining	43.3	17.6	11.6
0.009	0	0.009	880	-885	197	345552	Facets, 2 grains	79.8	20	900.8
0.009	0	0.009	879	-936	203	297171	Surface mark	21	3.4	0
0.009	0.0002	0.0088	871	-894	202	322526	Surface mark	77	8.3	0
0.009	0.0001	0.0089	892	-881	197	202310	Pore	21.6	21	48
0.009	0.0002	0.0088	890	-868	199	182449	Type II: Al-oxide	107	26.4	18
0.009	0	0.009	872	-879	196	366996	Facet	63.3	48	2269
0.009	0	0.009	882	-883	196	332160	Type II: S- rich	23	5	1625

Table 3 – *Summarized Resulting Disk Process/Location Relationships*

Test	R_ε=0	R_ε=-1	R_ε=0	
	$\Delta\varepsilon_t$=0.75%	$\Delta\varepsilon_t$=0.90%	$\Delta\varepsilon_t$=0.75%	
Response	Log N_f	Log N_f	$\sigma_{y0.1\%}$	Grain Size
Data Points	20	20	19	15
Model Terms	5	6	5	4
Disk(D)	+	-		
Radius(R)	-	-	+	-
Vertical(V)	+		-	
D*R	+	+		
D*V		+	+	
R*V		+		+
R**2			-	-
r^2_{adj}	0.319	0.458	0.534	0.444

Table 4 – *Comparison of Minimum Life Estimates For Different Distribution Assumptions*

Prime Test Condition	$\Delta\varepsilon_t$=0.75%, R_ε=0		$\Delta\varepsilon_t$=0.90%, R_ε=-1	
Data Points	20	19[1]	20	19[1]
Normal	-92821	-64671	27364	40018
Weibull	64760	145076	157945	160486
Log Normal	42774	67738	112143	119643
Lowest Life	53269	148743	182449	183923

Table 5 – *Comparison of Life Estimates Using General Life Equations*

Input Data: Gen. Equation Terms	rms	r^2_{adj}	$\Delta\varepsilon_t$=0.75%, R_ε=0		$\Delta\varepsilon_t$=0.90%, R_ε=-1	
	Stan.Dev		Mean Life	Min. Life	Mean Life	Min. Life
n=20, log normal life	0.193		198099	42774		
n=20, log normal life	0.117			42774	283985	112143
n=68: $1/\Delta\varepsilon_t^3$,R_ε,$R_\varepsilon/\Delta\varepsilon_t^3$	0.243	0.847	199883	33540	256965	43451
n=86: log $\Delta\varepsilon_t$,log σ_{max},log $\Delta\varepsilon_t$*log σ_{max}	0.3203	0.841	135981	13508	203728	20211
n=86: log σ_{SWT}	0.3313	0.829	128271	11955	184963	17252
n=86: log σ_{Walker}	0.3298	0.831	139449	13142	173157	16327
n=86: log $\Delta\varepsilon_{BCM}$	0.3460	0.816	143785	13172	215524	19744
n=67[1]: $1/\Delta\varepsilon_t^3$,R_ε,$R_\varepsilon/\Delta\varepsilon_t^3$	0.19	0.903	199883	49342	279428	69354
n=85[1]: log $\Delta\varepsilon_t$,log σ_{max},log $\Delta\varepsilon_t$*log σ_{max}	0.2912	0.866	136888	16762	219070	26775
n=85[1]: log σ_{SWT}	0.3065	0.851	132602	14752	191027	21267
n=85[1]: log σ_{Walker}	0.3062	0.852	144045	16065	178738	19943
n=85[1]: log $\Delta\varepsilon_{BCM}$	0.3191	0.841	143301	15810	215524	23778

[1]After removing low life outlier

Figure 1 – *Cluster Forging [5]*

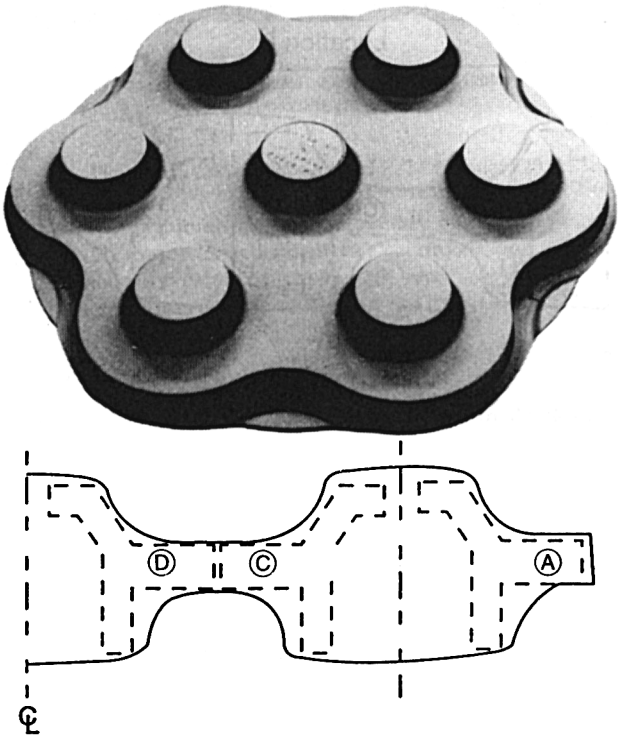

Figure 2 – *Typical Microstructure*

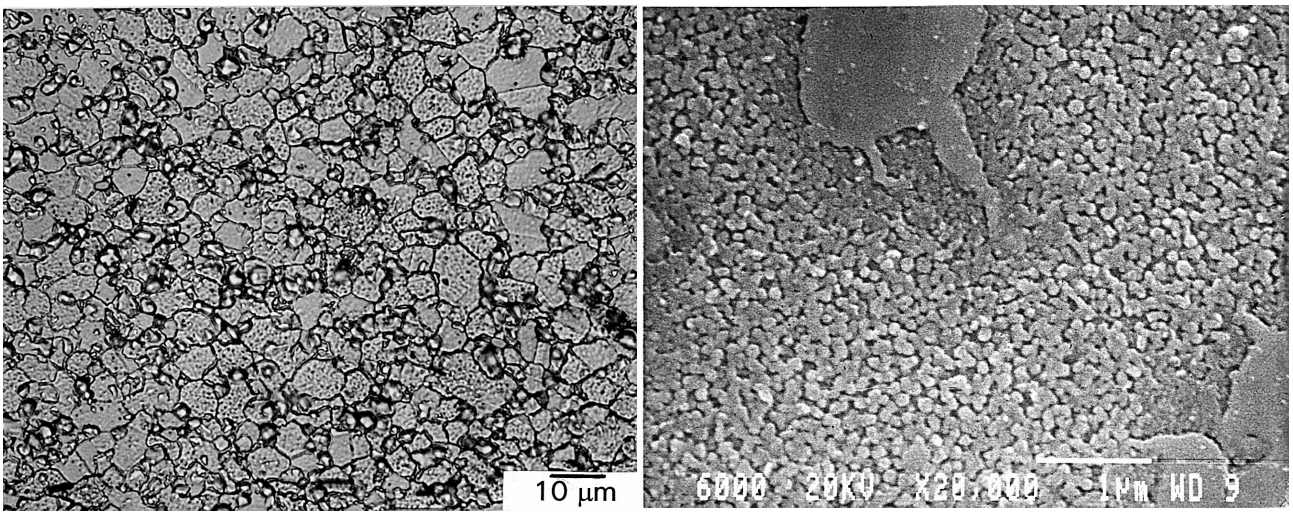

Figure 3 – *Typical Failure Initiation Sites at $\Delta\varepsilon_t$=0.75%, R_ε=0*

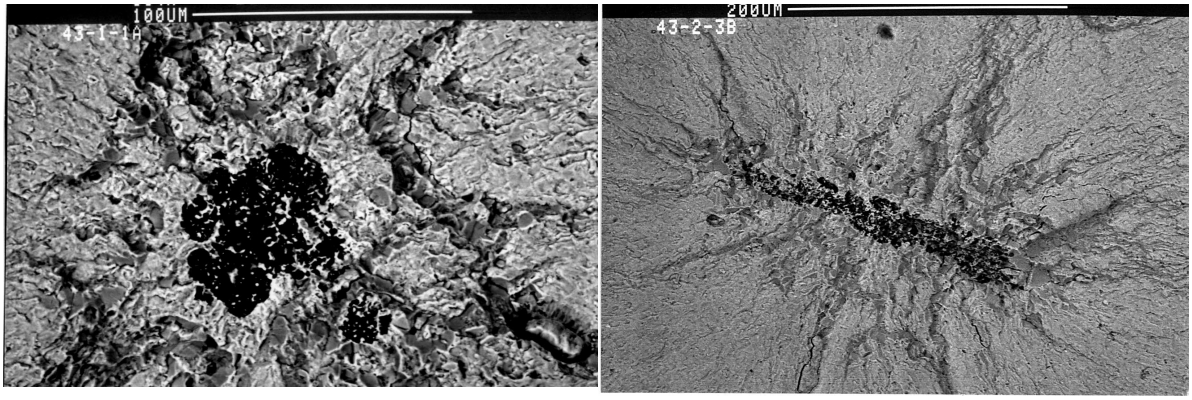

Figure 4 – *Typical Failure Initiation Sites at $\Delta\varepsilon_t$=0.90%, R_ε=-1*

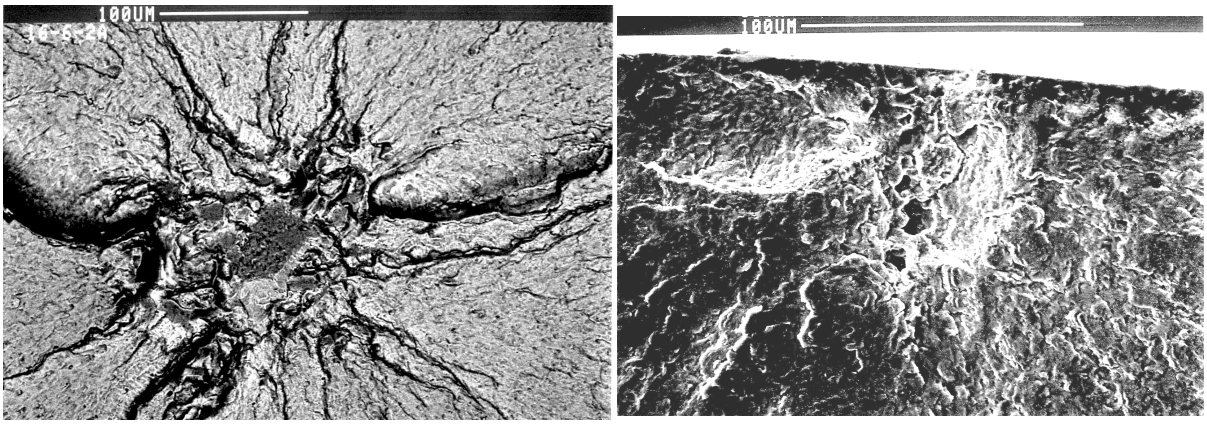

Figure 5 – *Scatter Plots of Lives vs. Processing/Location Variables*

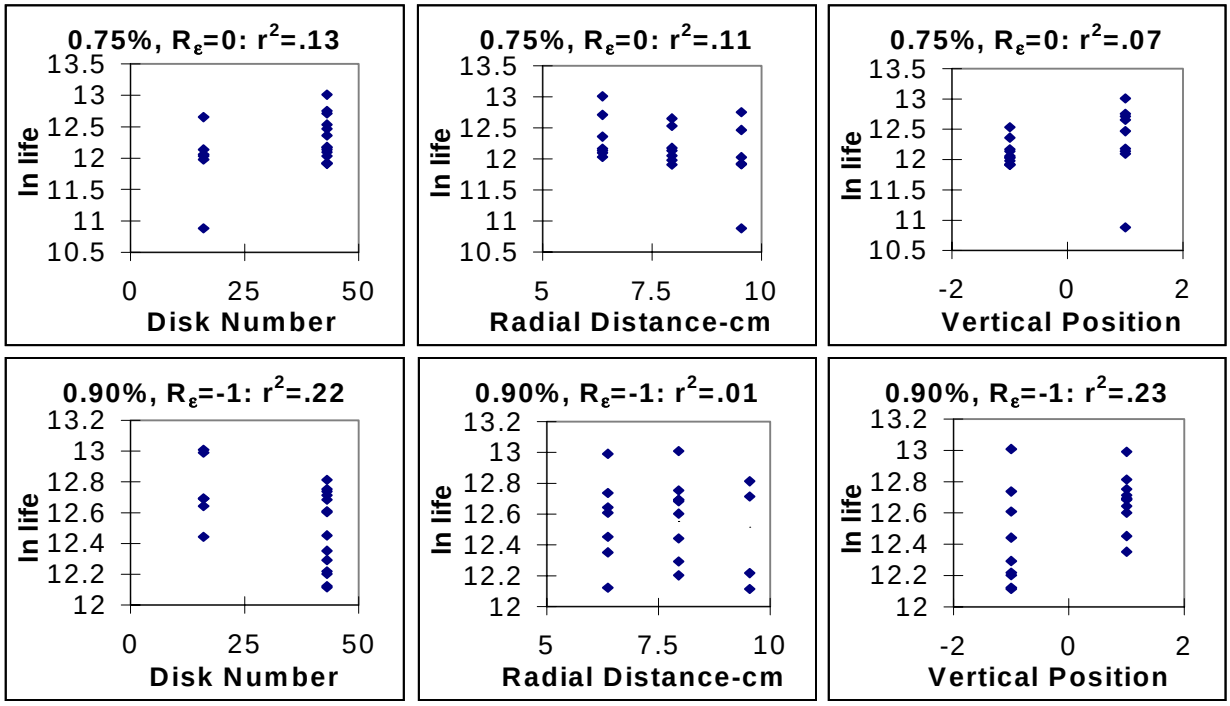

Figure 6 – *Probability Plots Using Normal and Weibull Distribution Assumptions*

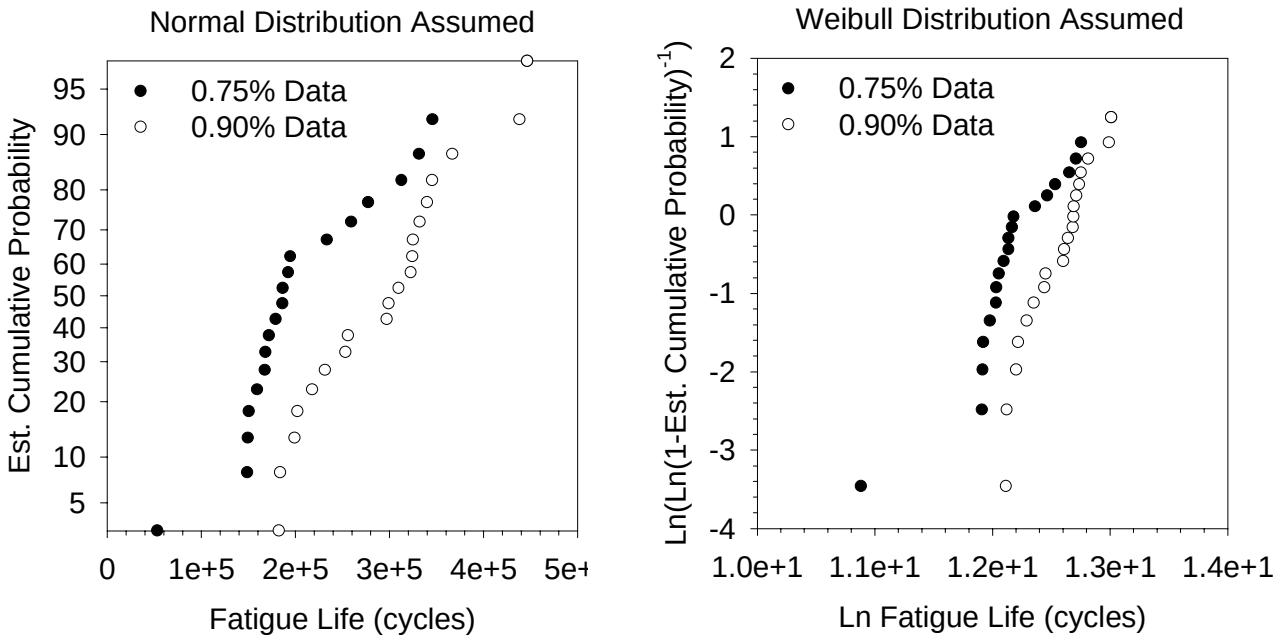

Figure 7 – *Probability Plot Using Log Normal Distribution Assumption*

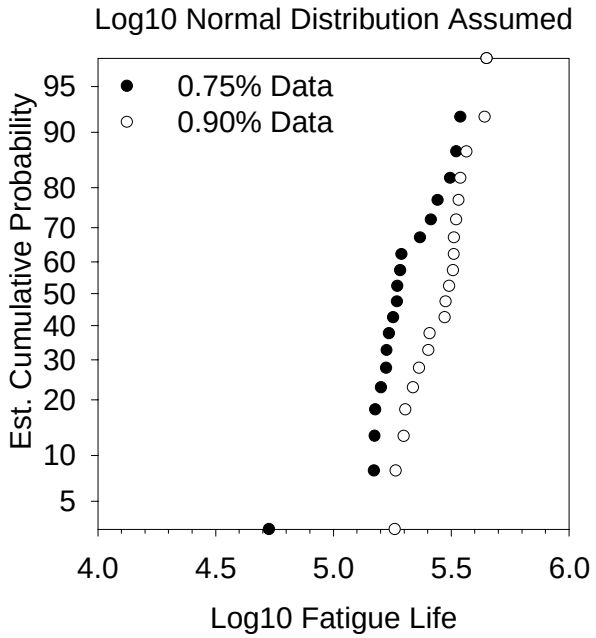

Figure 8 – *Minimum Life Estimates Using The Different Life Distribution Assumptions*

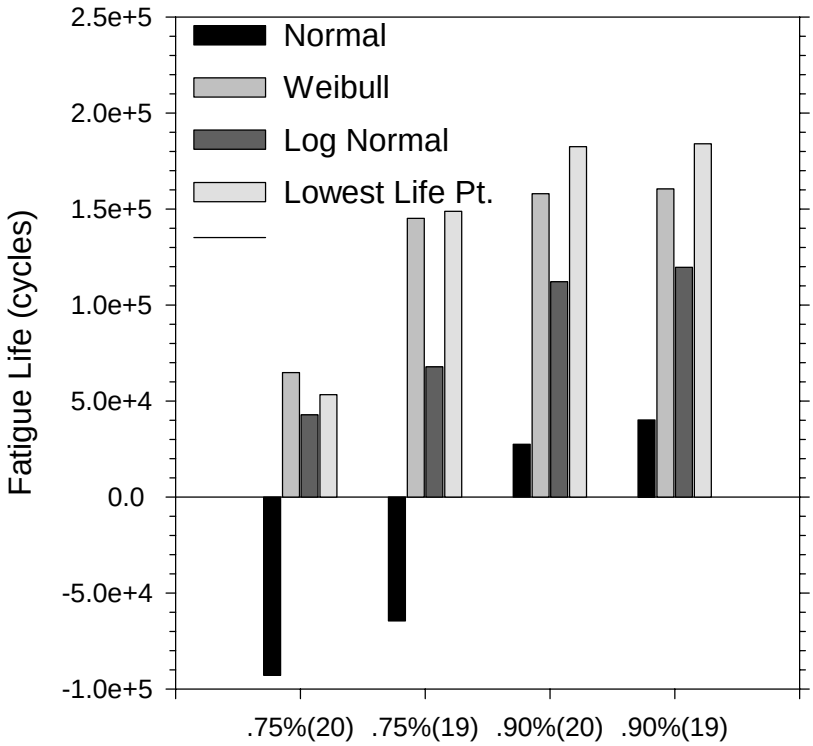

Figure 9 – *Comparison of Estimated and Actual Lives Using General Equations*

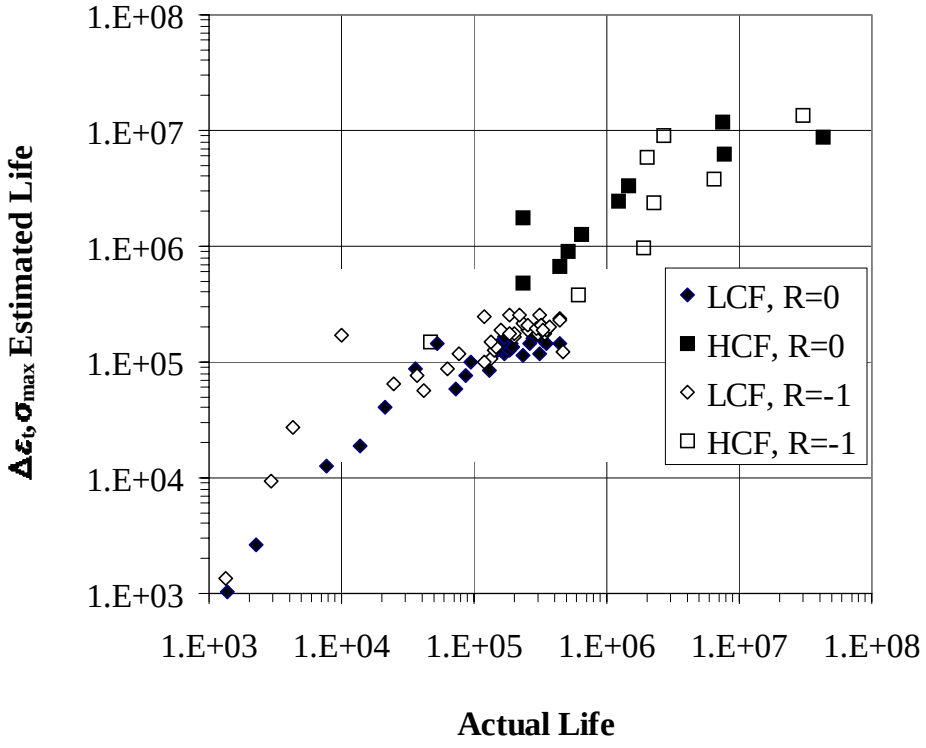

Figure 10 – *Comparison of Minimum Life Estimates Using General Equations at $\Delta\varepsilon_t$=0.75%, R_ε=0*

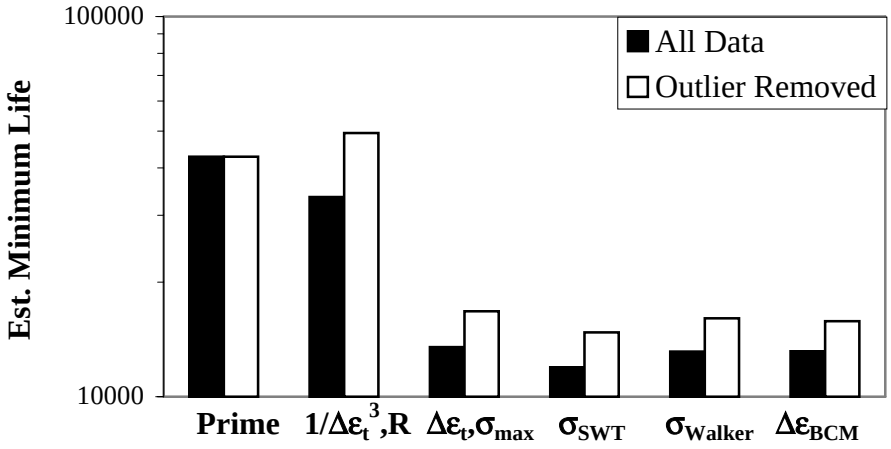

Figure 11 – *Comparison of Minimum Life Estimates Using General Equations at $\Delta\varepsilon_t$=0.90%, R_ε=-1*

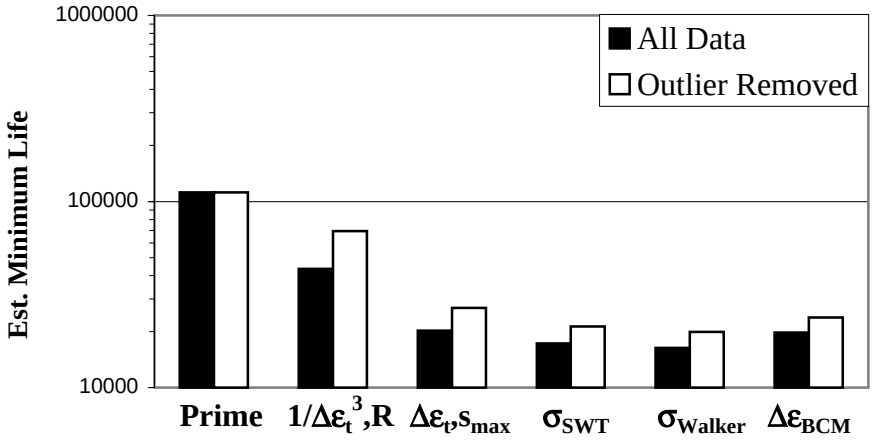

Figure 12 – *Scatter Plots of Life Versus Failure Defect Size and Depth*

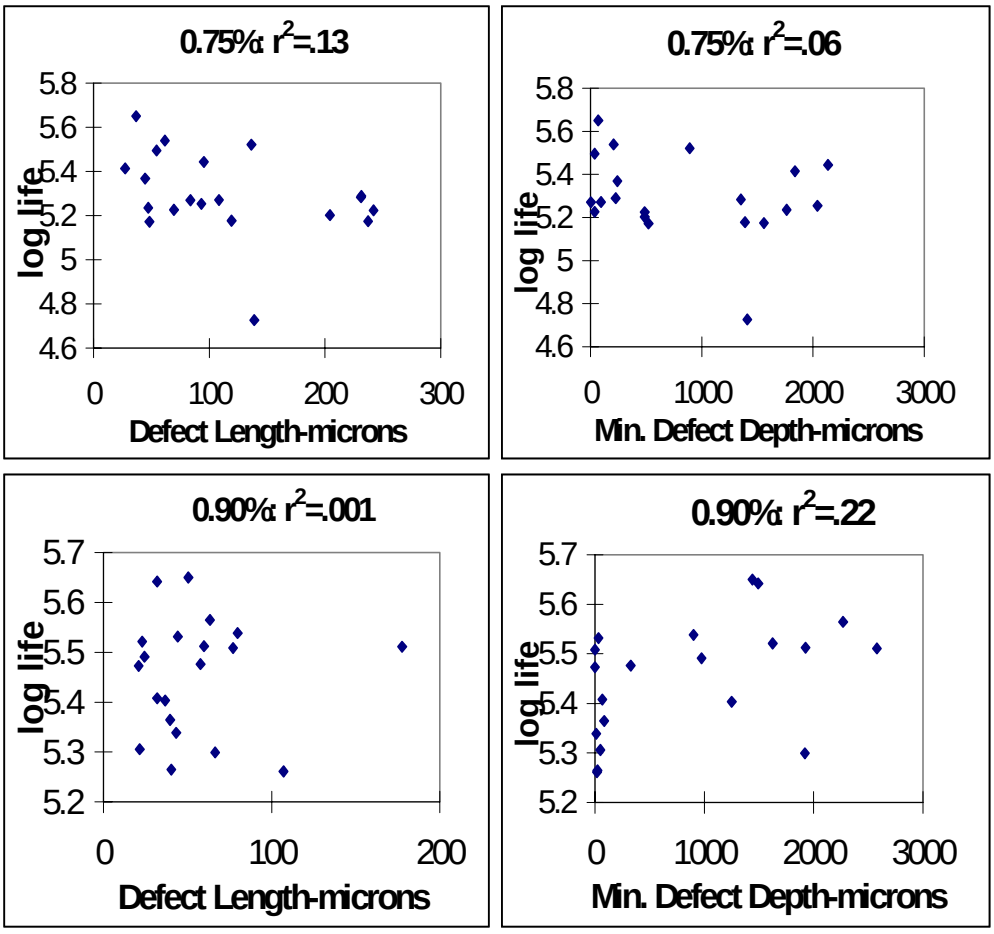

Figure 13 – *Comparison of Life and Initial Stress Intensity at Failure Initiation Points*

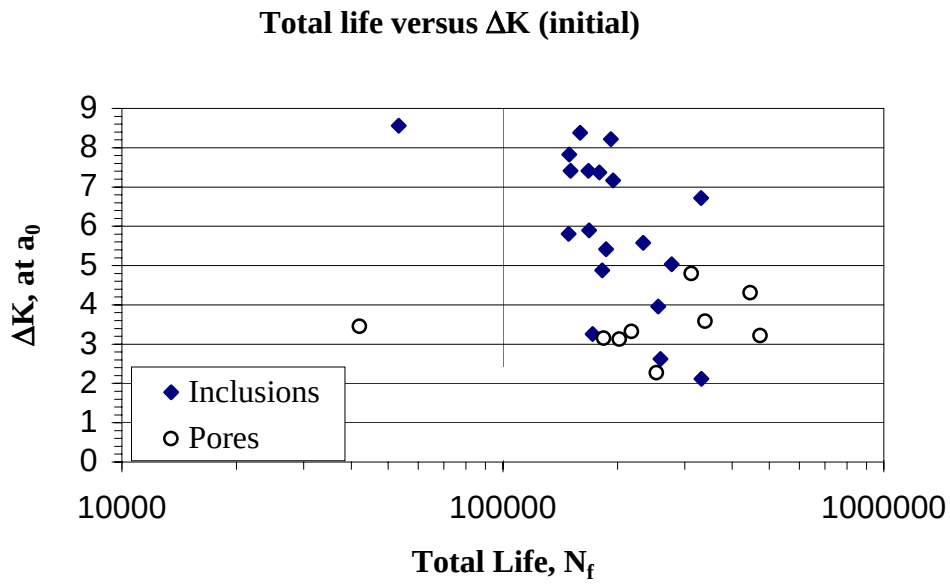

Figure 14 – *Calculated Crack Propagation Life Versus Initial Stress Intensity at Failure Initiation Points*

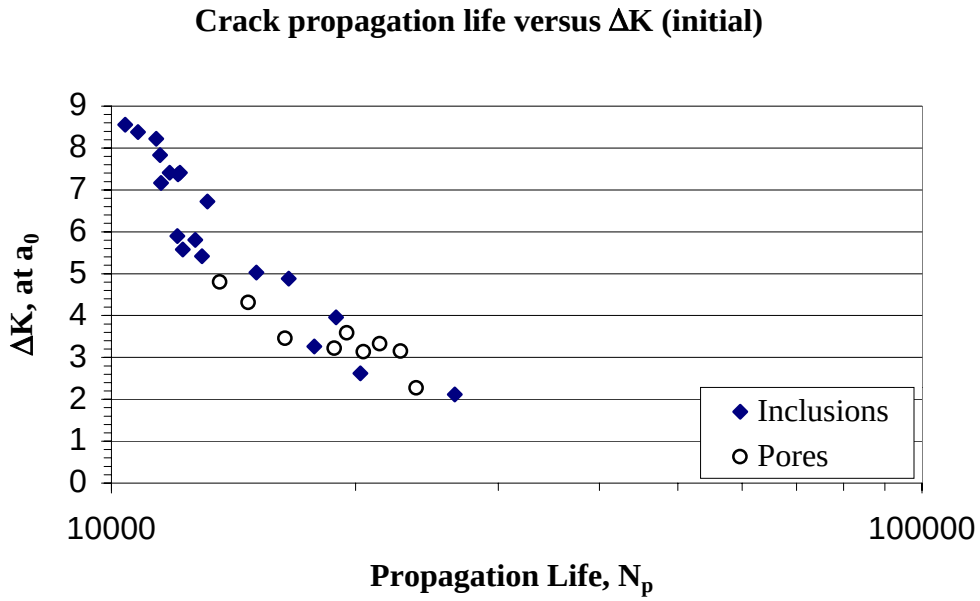

Figure 15 – *Calculated Crack Initiation Life Versus Initial Stress Intensity at Failure Initiation Points*

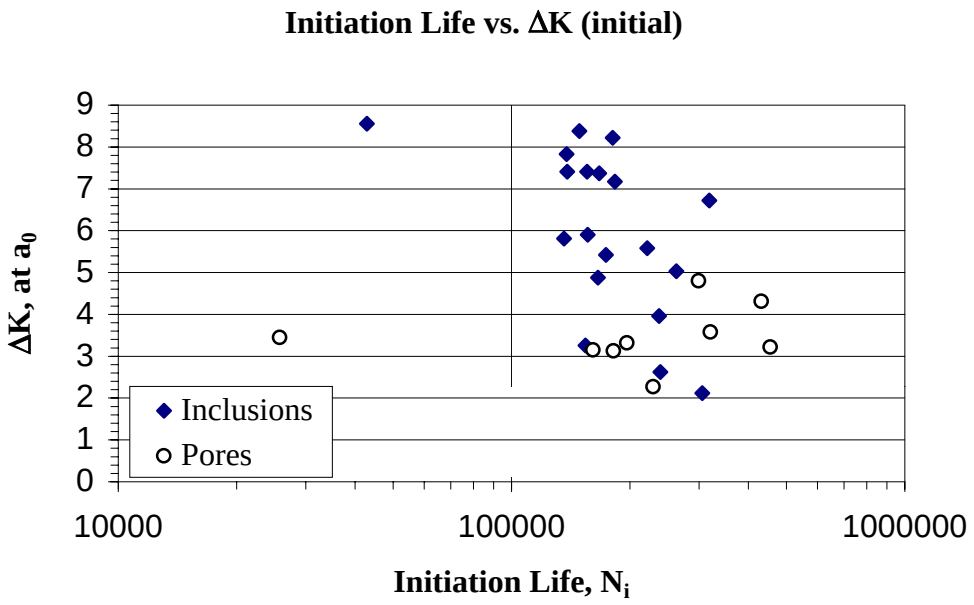

Figure 16 – *Calculated Percent Crack Initiation Life Versus Total Life*

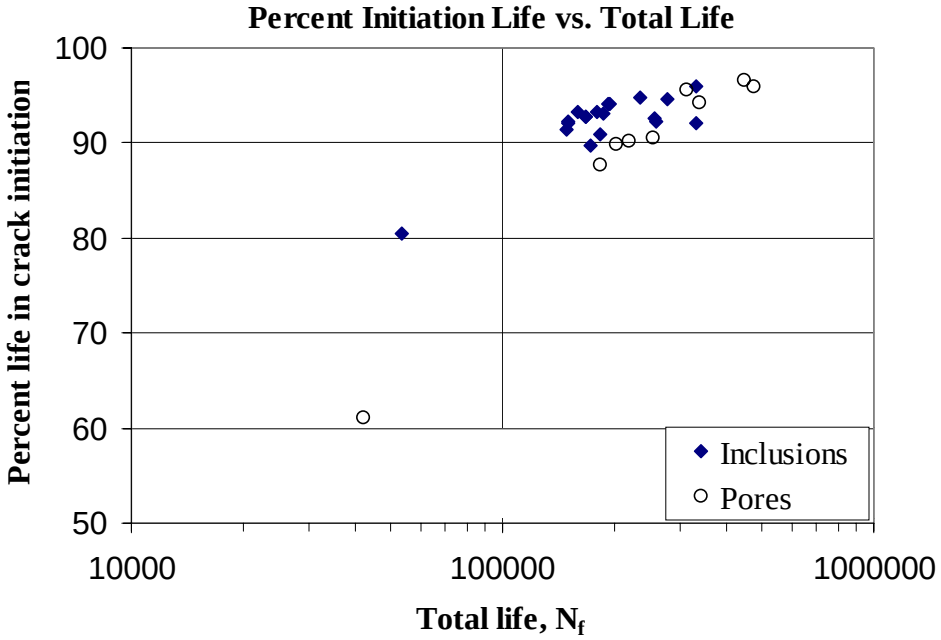

REPORT DOCUMENTATION PAGE

Form Approved
OMB No. 0704-0188

1. AGENCY USE ONLY (*Leave blank*)	2. REPORT DATE	3. REPORT TYPE AND DATES COVERED
	March 2000	Technical Memorandum

4. TITLE AND SUBTITLE

Assessments of Low Cycle Fatigue Behavior of Powder Metallurgy Alloy U720

5. FUNDING NUMBERS

WU–523–24–13–00

6. AUTHOR(S)

Timothy P. Gabb, Peter J. Bonacuse, Louis J. Ghosn, Joseph W. Sweeney, Amit Chatterjee, and Kenneth A. Green

7. PERFORMING ORGANIZATION NAME(S) AND ADDRESS(ES)

National Aeronautics and Space Administration
John H. Glenn Research Center at Lewis Field
Cleveland, Ohio 44135–3191

8. PERFORMING ORGANIZATION REPORT NUMBER

E–12061

9. SPONSORING/MONITORING AGENCY NAME(S) AND ADDRESS(ES)

National Aeronautics and Space Administration
Washington, DC 20546–0001

10. SPONSORING/MONITORING AGENCY REPORT NUMBER

NASA TM—2000-209418

11. SUPPLEMENTARY NOTES

Timothy P. Gabb, NASA Glenn Research Center; Louis J. Ghosn, currently with Eveready Battery Company, Inc., Westlake, Ohio; Peter J. Bonacuse, U.S. Army Research Laboratory, NASA Glenn Research Center; Joseph W. Sweeney, Gilcrest Electric Company, 3000 Aerospace Parkway, Brook Park, Ohio 44135; Amit Chatterjee and Kenneth A. Green, Allison Engine Company, Indianapolis, Indiana. Responsible person, Timothy P. Gabb, organization code 5120, (216) 433–3272.

12a. DISTRIBUTION/AVAILABILITY STATEMENT

Unclassified - Unlimited
Subject Categories: 26 and 39 Distribution: Nonstandard

This publication is available from the NASA Center for AeroSpace Information, (301) 621–0390.

12b. DISTRIBUTION CODE

13. ABSTRACT ***(Maximum 200 words)***

The fatigue lives of modern powder metallurgy disk alloys are influenced by variabilities in alloy microstructure and mechanical properties. These properties can vary as functions of variables the different steps of materials/component processing: powder atomization, consolidation, extrusion, forging, heat treating, and machining. It is important to understand the relationship between the statistical variations in life and these variables, as well as the change in life distribution due to changes in fatigue loading conditions. The objective of this study was to investigate these relationships in a nickel-base disk superalloy, U720, produced using powder metallurgy processing. Multiple strain-controlled fatigue tests were performed at 538 °C (1000 °F) at limited sets of test conditions. Analyses were performed to: (1) assess variations of microstructure, mechanical properties, and LCF failure initiation sites as functions of disk processing and loading conditions; and (2) compare mean and minimum fatigue life predictions using different approaches for modeling the data from assorted test conditions. Significant variations in life were observed as functions of the disk processing variables evaluated. However, the lives of all specimens could still be combined and modeled together. The failure initiation sites for tests performed at a strain ratio $R_\varepsilon = \varepsilon_{min}/\varepsilon_{max}$ of 0 were different from those in tests at a strain ratio of –1. An approach could still be applied to account for the differences in mean and maximum stresses and strains. This allowed the data in tests of various conditions to be combined for more robust statistical estimates of mean and minimum lives.

14. SUBJECT TERMS

Superalloy; Powder metallurgy; Low cycle fatigue; Inclusions; Facets

15. NUMBER OF PAGES

26

16. PRICE CODE

A03

17. SECURITY CLASSIFICATION OF REPORT	18. SECURITY CLASSIFICATION OF THIS PAGE	19. SECURITY CLASSIFICATION OF ABSTRACT	20. LIMITATION OF ABSTRACT
Unclassified	Unclassified	Unclassified	